Author(s): Juarez Mosqueda, Rosalba; Malola, Sami; Häkkinen, Hannu

Title: Stability, electronic structure, and optical properties of protected gold-doped silver Ag29-xAux (x = 0-5) nanoclusters

Year: 2017

Version:

Please cite the original version:

Juarez Mosqueda, R., Malola, S., & Häkkinen, H. (2017). Stability, electronic structure, and optical properties of protected gold-doped silver Ag29-xAux (x = 0-5) nanoclusters. Physical Chemistry Chemical Physics, 19(21), 13868-13874. https://doi.org/10.1039/C7CP01440F

PCCP

Accepted Manuscript

This article can be cited before page numbers have been issued, to do this please use: R. Juarez-Mosqueda, S. Malola and H. Häkkinen, *Phys. Chem. Chem. Phys.*, 2017, DOI: 10.1039/C7CP01440F.

ROYAL SOCIETY OF CHEMISTRY

rsc.li/pccp

View Article Online
DOI: 10.1039/C7CP01440F

Stability, electronic structure, and optical properties of protected gold-doped silver $Ag_{29-x}Au_x$ (x = 0-5) nanoclusters

Rosalba Juarez-Mosqueda,[†] *Sami Malola,*[†] *and Hannu Häkkinen*[*†‡]

[†]Department of Physics and [‡]Department of Chemistry, Nanoscience Center, University of Jyväskylä, FI-40014 Jyväskylä, Finland

ABSTRACT: In this work we used density functional theory (DFT) and linear response time-dependent DFT (LR-TDDFT) to investigate the stability, electronic structure, and optical properties of Au-doped $[Ag_{29-x}Au_x(BDT)_{12}(TPP)_4]^{3-}$ nanoclusters (BDT:1,3-benzenedithiol; TPP triphenylphosphine) with x=0-5. The aim is to shed light on the most favorable doped structures by comparing our results with previously published experimental data. The calculated relative energies, ranging between 0.8-10 meV/atom, indicate that several doped $Ag_{29-x}Au_x$ nanoclusters are likely to co-exist at room temperature. However, only the Au-doped $[Ag_{29-x}Au_x(BDT)_{12}(TPP)_4]^{3-}$ nanoclusters that have direct bonding between Au dopants and phosphines display an enhancement in the electronic transitions at ~450 nm. This agrees with the main spectral absorption features that have been experimentally reported for the mixture of Au-doped silver $Ag_{29-x}Au_x$ nanoclusters. In addition, the formation of Au-TPP bonding could prevent cluster degradation starting from the detachment of the phosphine molecules, since the Au-TPP

View Article Online
DOI: 10.1039/C7CP01440F

bond is stronger by ~0.4 eV than the analogous Ag-TPP one. Thus, the results presented here show the important role of the Au-TPP bonding in determining the stability and optical properties of thiolate-phosphine-protected $Ag_{29-x}Au_x$ nanoclusters.

INTRODUCTION

Several Ag-based nanoclusters stabilized by polymers[1], dendrimers,[2] peptides,[3] proteins,[4] or stranded DNA,[5–8] display remarkable luminescence properties that render them promising for biolabeling,[9] sensing,[1,10] and bioimaging.[3,4,9,11,12] Nonetheless, the luminescence of such materials is strongly sensitive to the conformational structure and/or sequence of the protecting biomolecules.[7,13] On the other hand, the synthesis of stable silver nanoclusters protected with smaller molecules, such as thiols, has been challenging and only done fifteen years after the synthesis of the first thiolate-capped gold nanocluster.[14–16]

Recently, the groups of Bakr and Zheng have implemented an interesting strategy to stabilize thiolate-protected silver nanoclusters based on the use of a mixture of thiols and phosphines as protecting agents.[17–19] With this approach, they have successfully synthesized silver nanoclusters with non-magic superatomic electronic configurations[17] and non-spherical shapes.[17–19] They found that in such materials the phosphines attach to the outermost layer forming an additional protecting shell.[17–21] The group of Bakr also reported that the incorporation of Au dopants to the thiolate-phosphine-protected Ag_{29} nanocluster significantly enhance the cluster stability, and surprisingly, its photoluminescence quantum yield.[21]

According to the mass spectrometry measurements, the Au-doped silver nanoclusters synthesized in the group of Bakr have molecular masses that correspond to $[Ag_{29-x}Au_x(BDT)_{12}(TPP)_4]^{3-}$ structures mainly with x=1-5. Furthermore, the P NMR analysis suggests that Au dopants bond to phosphines.[21] While the determination of the crystal structure of

View Article Online
DOI: 10.1039/C7CP01440F

$[Ag_{29}(BDT)_{12}(TPP)_4]^{3-}$ and $[Ag_{29}Au(BDT)_{12}(TPP)_4]^{3-}$ has been achieved,[21] the structure of the Au-doped nanoclusters with $2 \leq x \leq 5$ remains unknown. As a consequence, the source of the enhancement of the photoluminescence quantum yield has still not been clarified.

The aim of this work is to unveil the molecular structure of the energetically-most favorable and likely Au-doped $[Ag_{29-x}Au_x(BDT)_{12}(TPP)_4]^{3-}$ nanoclusters present in the synthesized samples.[21] For that purpose, we calculate and compare the ground states energies of different $[Ag_{29-x}Au_x(BDT)_{12}(TPP)_4]^{3-}$ nanoclusters with x=0-5 by using DFT calculations. Additionally, we calculate the optical spectra of the pristine and doped nanoclusters and contrast them with the experimental data.[21] The calculated energy differences, ranging from 0.8-10 meV/atom, suggest that several Au-doped $[Ag_{29-x}Au_x(BDT)_{12}(TPP)_4]^{3-}$ isomers could to co-exist in the synthesized mixture of products. These energy differences per atom are of the same order of magnitude as difference between the energy of the *fcc* (face-centred cubic) Au and the metastable *hcp* (hexagonal close-packed) Au phases.[22–26] Moreover, the comparison between the calculated and the experimental optical spectra indicates that main absorption features, such as the broadening and the blue-shift of the characteristic Ag_{29} peak (at 447 nm), of the experimental spectra result from the contributions of the diverse Au-doped isomers co-existing in the synthesized mixture. Particularly, the blue-shifting is due to the presence of nanoclusters whose molecular structure contains direct Au-TPP bonding.

COMPUTATIONAL METHODS

A set of Au-doped $[Ag_{29-x}Au_x(BDT)_{12}(TPP)_4]^{3-}$ nanoclusters with x = 2-5 were built from the atomic coordinates of the experimental $[Ag_{29}(BDT)_{12}(TPP)_4]^{3-}$ and $[Ag_{28}Au(BDT)_{12}(TPP)_4]^{3-}$ crystal structures provided by Bakr.[20,21] According to the total electron count formula introduced

View Article Online
DOI: 10.1039/C7CP01440F

by introduced by Häkkinen and collaborators[27] all the studied nanoclusters are 8-electrons closed-shell structures. **Figure 1** illustrates the structure of a $[Ag_{29-x}Au_x(BDT)_{12}(TPP)_4]^{3-}$ nanocluster and its different shells (*S0*-*S3*) that can be occupied by the Au dopants.

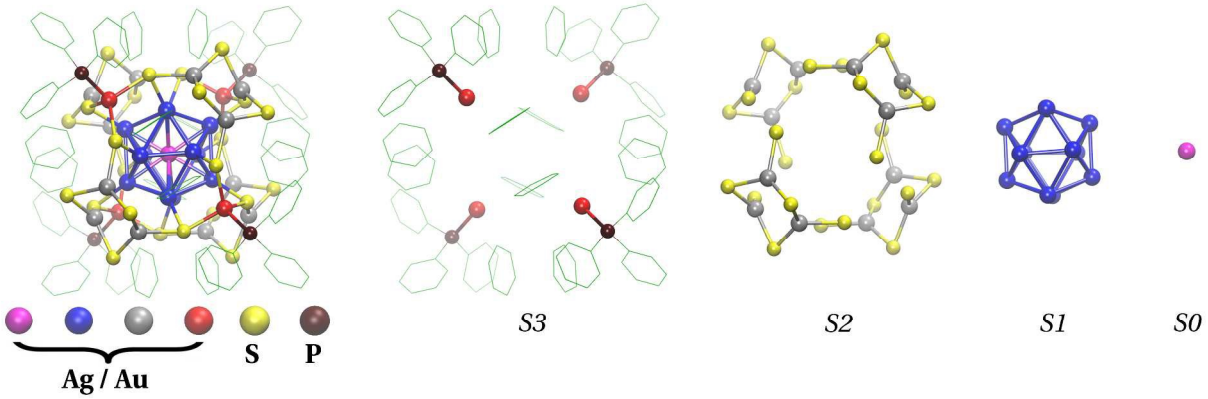

Figure 1. Representation of a $[Ag_{29-x}Au_x(BDT)_{12}(TPP)_4]^{3-}$ nanocluster and its different shell structures (*S3*-*S0*). Color code: violet, the noble metal atom (Ag or Au) located at the center of the cluster (*S0*). Blue, the metal atoms at the first shell (*S1*). Gray, and red, the Ag and/or Au atoms at the second (*S2*) and third shell (*S3*), respectively. Phosphorus is shown in brown and sulfur in yellow. Phenyl rings are drawn in green and hydrogen atoms have been removed for clarity

The experimental and built nanocluster structures were optimized in a cubic box with a grid spacing of 0.2 Å. All the calculations were carried out by using the real-space code-package GPAW (grid-based projector-augmented wave method).[28,29] The optimizations and electronic structure calculations were performed in the frame of density functional theory (DFT) by using the generalized gradient-corrected PBE[30] functional. The van der Waals vdW-DF-CX[31,32] functional was also used to compare the ground state energies and geometries with the ones obtained from the PBE calculations. The convergence criterion for the forces acting on individual atoms was set to a maximum value of 0.05 eV/Å.

The optical spectra were calculated by using Casida´s formulation of linear response time dependent DFT (LR-TDDFT).[33,34] The electronic transitions were analyzed based on the time-

View Article Online
DOI: 10.1039/C7CP01440F

dependent density functional perturbation theory (TD-DFPT)[35] following the method reported earlier by Malola *et al*.[36] The Kohn-Sham wave functions were projected onto the spherical harmonic (Y_{lm}) basis by using the cluster and the atomic radial cutoffs of 11.5 Å, for the cluster, and 0.85 Å for C, 1.40 Å for Ag and Au, and 1.1 Å for P and S. The overlap integrals were broadened (with a Gaussian function of width = 0.01 eV) and plotted as projected local density of states (PLDOS) per cluster and per atom. The atomic charges were calculated by using the Bader charge analysis.[37]

RESULTS AND DISCUSSION

In tables 1 and S1 (see Supplementary Information, SI), we show the set of $[Ag_{29-x}Au_x(BDT)_{12}(TPP)_4]^{3-}$ nanoclusters studied in this work. The relative energies of each cluster are calculated with respect to its lowest-energy isomer. The results from both the PBE and van der Waals functionals demonstrate that nanoclusters doped at the inner shells, *S0* and *S1*, are energetically more stable compared to structures in which Au atoms are at the *S2* and/or *S3* shells. Nevertheless, the energy difference between the calculated isomers range between 0.243-3.085 eV, that is 0.8-10 meV/atom (considering the 309 atoms constituting the nanoclusters). The most extreme cases are the structures of type **xA** and **xD**. In the former one, all of the 1-5 Au atoms are at the innermost shells forming the energetically most stable structures, and in the latter one, 1-4 of the Au dopants are at the outermost shell having higher energy structures. According to DFT-based calculations, the energy difference between *fcc-hcp* and *fcc-bcc* phases of gold and silver are between 0.6-3.4 meV/atom[22–25] and 19-23 meV/atom,[22] respectively. Moreover, the *hcp* Au phase, which is stable under ambient conditions, transform to *fcc* phase on exposure to a transmission electron microscope beam.[26] This might suggest that in the mixture of

View Article Online
DOI: 10.1039/C7CP01440F

Au-doped $[Ag_{29-x}Au_x(BDT)_{12}(TPP)_4]^{3-}$ nanoclusters, several isomers are energetically favorable to co-exist at room temperature.

The values of the HOMO-LUMO energy gaps shown in tables 1 and S1, indicate that having Au dopants at the outermost shell of the cluster, as it is in the **1D**, **2D**, **3D**, and **4D** structures, leads to a drop of ~70 meV in the HOMO-LUMO energy gap when compared to the analogous **xA** isomers. The decrease in the HOMO-LUMO energy gap was also observed by Soldan *et al*. as a red-shift in the lower-energy edge of the UV/Vis spectra of the Au-doped samples.[21]

Table 1. Relative energies and HOMO-LUMO energy gap (given in parentheses) of $[Ag_{29-x}Au_x(BDT)_{12}(TPP)_4]^{3-}$ nanoclusters with x=0-5. The formula $Ag_{29-x}Au_x@Sn$ indicates the number of Au atoms (x) at each cluster shell (*Sn*), *n* being from 0 to 3. **xA-xD** are the labeling to specify the number of Au dopants and the type of structure. The **Ag_{29}** label is used to refer to the undoped nanocluster. Values in bold correspond to the relative energies and HOMO-LUMO energy gaps calculated with the van der Waals functional. All energies are expressed in eV per cluster.

Label	**Ag_{29}**	**xA**	**xB**	**xC**	**xD**	
	$Ag_{29-x}Au_x$	**$Ag_{29-x}Au@S0$-$Au_{x-1}@S1$**	**$Ag_{29-x}Au_x@S1$**	**$Ag_{29-x}Au_x@S2$**	**$Ag_{29-x}Au_x@S3$**	**$Ag_{29-x}Au@S0$-$Au_{x-1}@S3$**
x = 0	0.000 (1.786) **0.000 (1.719)**	----	----	----	----	----
x = 1	----	0.000 (1.833) **0.000 (1.744)**	0.332 (1.765) **0.305 (1.681)**	0.601 (1.808) **0.192 (1.631)**	0.718 (1.762) **0.262 (1.652)**	----
x = 2	----	0.000 (1.844)	0.346 (1.723)	0.811 (1.785)	1.189 (1.774)	----
x = 3	----	0.000 (1.820) **0.000 (1.738)**	0.336 (1.735) **0.377 (1.667)**	1.079 (1.780) **1.411 (1.680)**	1.575 (1.755) **2.051 (1.657)**	----
x = 4	----	0.000 (1.804)	0.312 (1.715)	1.119 (1.870)	1.919 (1.737)	----
x = 5	----	0.000 (1.784) **0.000 (1.717)**	0.299 (1.673) **0.347 (1.634)**	1.502 (1.792) **2.200 (1.602)**	----	1.499 (1.791) **3.085 (1.691)**

To understand the bonding mechanism we calculated the strength of the Au-TPP and Ag-TPP bonding in structures **5A** and **5D** according to the equation $[Ag_{29-x}Au_x(BDT)_{12}(TPP)_4]^{3-} \rightarrow$

View Article Online
DOI: 10.1039/C7CP01440F

$[Ag_{29-x}Au_x(BDT)_{12}(TPP)_3]^{3-}$ + TPP. From these calculations we found that the Au-P bond is ~ 0.4 eV stronger than the Ag-P one. Thus, the formation of bonds between the Au dopants and the phosphines could largely explain the enhanced stability observed in the Au-doped samples. However, it is worth to point out that the increase of the stability is not exclusively caused by the Au-TPP bonding, but also by the Au doping at innermost shells as shown in Table 1. Besides, the formation of Au-SR bonding by doping at the *S2* shell could also contribute to the enhancement of the cluster stability since the interaction between gold and thiols is known to be stronger than in the case of silver.[38]

According to the results obtained from the Bader charge analysis (see **Table S2**), the atomic charge on each atom remains almost unaffected by the number and the location of Au atoms within the cluster. Nevertheless, the largest variation (0.212 a.u.) is observed in the atomic charge of P from the reference TPP molecule (with atomic charge 1.382 a.u. on P) to the **3D** structure (where the atomic charge of P is 1.594 a.u.), which has three TPP molecules attached to the Au dopants. This suggest that there is a slightly more charge transfer from phosphorous to the rest of the molecule through Au-P bonding compared to the Ag-P one. This could also give insight into the shifting of the P NMR signal that has been observed for the mixture of $Ag_{29-x}Au_x$ nanoclusters.[21]

In **Figure 2**, we show the optical spectra of the $[Ag_{29-x}Au_x(BDT)_{12}(TPP)_4]^{3-}$ nanoclusters, with x=0-5, for the structures of type **xA** and **xD**. The comparison between both sets of spectra reveals that for the structures with Au-TPP bonding, **xD**, a third absorption peak appears at ~450 nm which is not observed in the spectra of the corresponding isomers with structure **xA**. To have a more complete picture, we also calculated the absorption spectra of the

View Article Online
DOI: 10.1039/C7CP01440F

$[Ag_{26}Au_3(BDT)_{12}(TPP)_4]^{3-}$ nanoclusters with structures **3B**, **3C**, **3F**, and **3H** (see **Figure 3** and **Figure S4**).

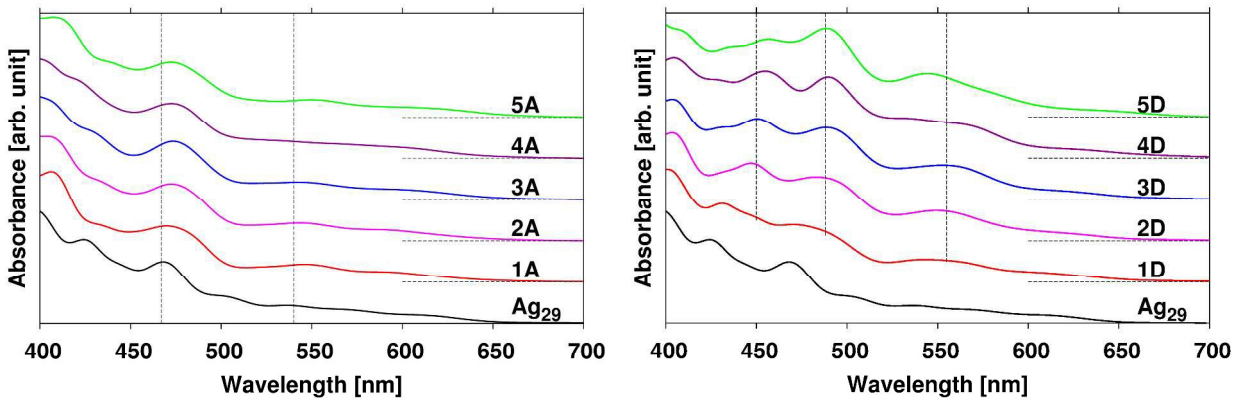

Figure 2. Optical spectra of the $[Ag_{29-x}Au_x(BDT)_{12}(TPP)_4]^{3-}$ nanoclusters with x = 0-5. In the doped nanoclusters the xAu atoms are at, the innermost shells *S0* and *S1* (**xA**), at the shell *S3* (**1D**, **2D**, **3D**, and **4D**), or at the shells *S0* and *S3* (**5D**).Vertical dashed lines are used to roughly indicate (from right to left) the position of the first, second, and third peaks. For comparison in **Figure S1**, we show the PBE absorption spectra of the $[Ag_{29}(BDT)_{12}(TPP)_4]^{3-}$ and $[Ag_{28}Au(BDT)_{12}(TPP)_4]^{3-}$ structures obtained from the experimental crystal analysis and from the PBE, vdW-DF-CX ground states calculations.

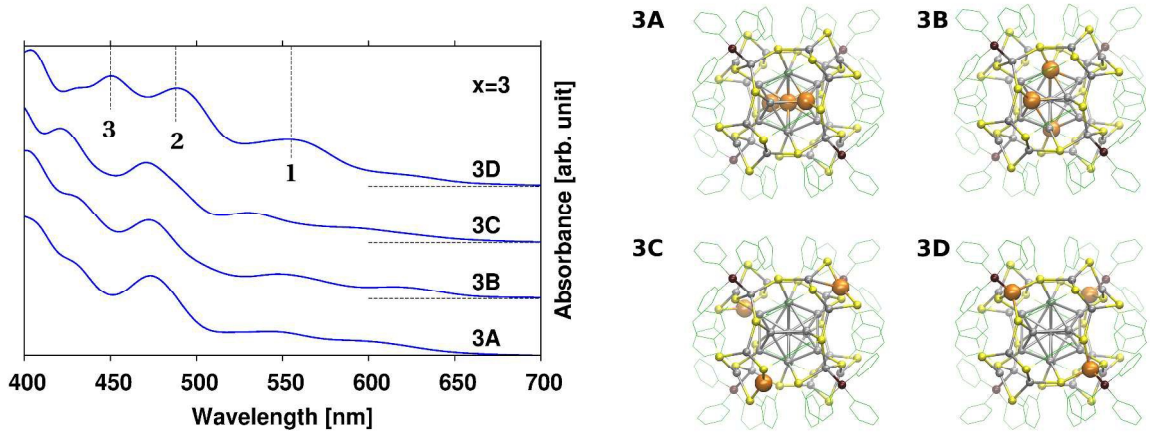

Figure 3. Optical spectra of the $[Ag_{26}Au_3(BDT)_{12}(TPP)_4]^{3-}$ nanoclusters with structures **3A**, **3B**, **3C**, and **3D** depicted at the right side. Vertical dashed lines are used to indicate the position of the first (555 nm), second (488 nm) and third absorption peak (450 nm) of the **3D** structure. Orange, gray, brown and yellow spheres represent Au, Ag, P and S atoms, respectively.

View Article Online
DOI: 10.1039/C7CP01440F

As shown in figures 3 and S4, the third absorption peak ~450 nm appears only in the optical spectra of the structures that contain Au-TPP bonding, and in the case of $[Ag_{26}Au_3(BDT)_{12}(TPP)_4]^{3-}$ nanoclusters it is the closest to the second one (the characteristic peak of Ag_{29}) in the spectrum of the **3D** structure. As reported by Soldan *et al.,*[21] the mass spectrometry and UV-vis measurements reveal that at 10-40% of Au precursor concentration different doped $[Ag_{29-x}Au_x(BDT)_{12}(TPP)_4]^{3-}$ nanoclusters appear in the mass spectra and produce a blue-shift and a broadening of the characteristic absorption peak of Ag_{29} at 447 nm. According to our results shown in figures 2,3, and S4, we suggest that the blue-shift of the main absorption peak that has been experimentally observed is mainly a consequence of the appearance of the absorption peak at ~450 nm in the spectra of the nanoclusters that contain Au-TPP bonding. Moreover, the intensity of this peak increases with the number of Au-TPP bonds, *e.g.* from structure **3H** (with one Au-TPP bond) to **3D** (with three Au-TPP bonds), as shown in **Figure S4**. According to PBE calculations, the relative energies of the structures **3H**, **3F**, and **4F**, which also contain Au-TPP bonding, are significantly smaller than for their corresponding **3D** and **4D** isomers (*c.f.* tables 1 and S1). These results indicate that the Au-TPP bonding is not exclusive of the high energy **xD** structures, and that species with lower energies could contribute significantly to the observed blue-shifting of the main absorption peak. On the other hand, based on the small energy differences between the Au doped isomers we suggest that the broadening of the peak in the experimental absorption spectra of the Au-doped samples results from the contributions from all nanoclusters co-existing in the synthesized mixture of products. Thus, our results support the statement made by experimentalists[21] that among the possible synthesized nanoclusters there are species with chemical structure that contain direct Au-TPP bonding.

View Article Online
DOI: 10.1039/C7CP01440F

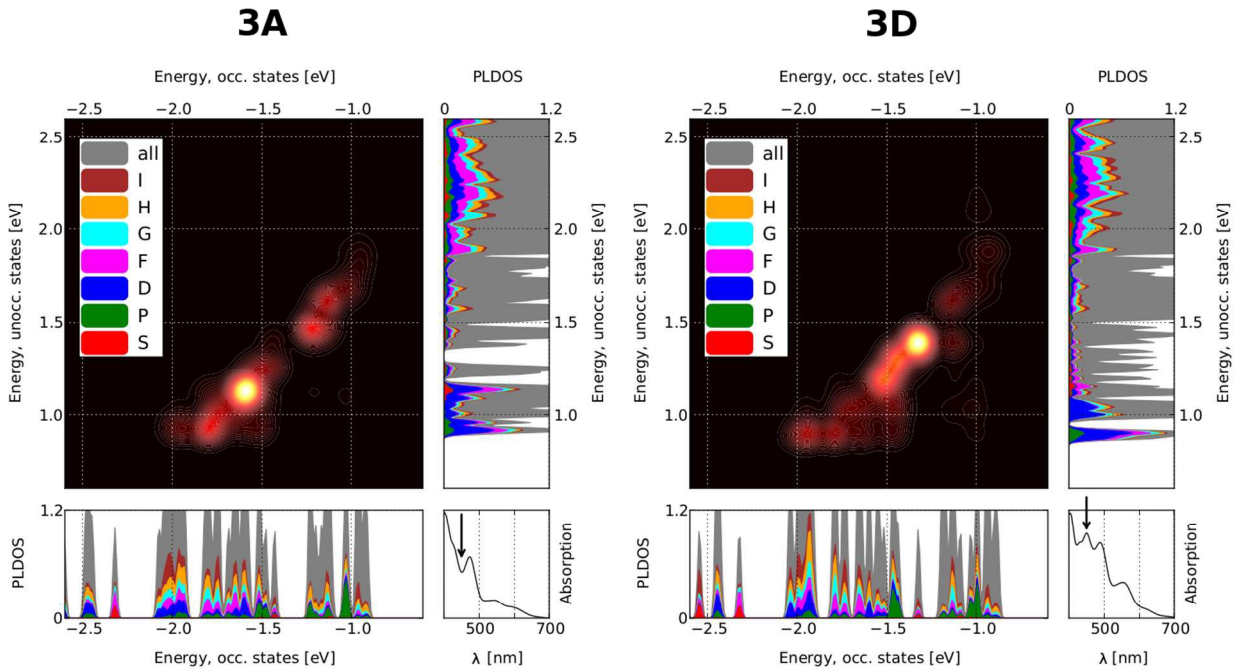

Figure 4. Transition contribution map for the spectral features of the $[Ag_{26}Au_3(BDT)_{12}(TPP)_4]^{3-}$ nanoclusters with structures **3A** and **3D**. The electronic transitions are analyzed at 450 nm for both the **3A** and **3D** structures. The angular-momentum-resolved (Y_{lm}) PLDOS of the occupied (bottom-left) and unoccupied (top-right) KS states are shown below and next to the TCM. The arrows in the optical spectra (bottom-right) point to the analyzed absorption peak.

To identify the energy range of the electronic transitions associated to the main absorption peaks, we analyzed the spectral features of the **3A** and **3D** structures using transition contribution maps (TCMs) (see **Figure 4** and **Figure S2** in SI). We found that in both **3A** and **3D** structures the transitions related to the first two peaks at 543-555 nm and 472-488 nm are mainly originated from the occupied states at around -1.20 eV to the unoccupied states at ~1.20–1.40 eV (see **Figure S2**). However, at 450 nm the most intense electronic transitions occur between different states in the **3A** and **3D** structures. While, in the case of the **3A** structure the most intense electronic transitions arise from the occupied states at around -1.60 eV to the unoccupied states

View Article Online
DOI: 10.1039/C7CP01440F

at 1.20 eV, in the **3D** structure they occur from the states at -1.32 eV to the states at 1.39 eV (see **Figure 4**).

To distinguish between the atomic orbitals involved in the electronic transitions at ~450 nm, we analyzed the PLDOS per atom (and per phenyl ring) for the **3A**, **3C**, and **3D** structures (see **Figures 5**). The results demonstrate that the occupied and unoccupied states at -1.32 eV and 1.39 eV are formed mainly by the local states of gold with p, d, and s character. Conversely, in the **3A** structure the Au(p,d) and Au(s) states are absent at that energy values. In the case of the **3C** structure the unoccupied Au(s) states are shifted to higher energy. These results suggest that the p, d, and s states of gold appearing at around -1.32 eV and 1.39 eV play an important role in the enhancement of the electronic transitions observed at ~450 nm in the spectra of structures with Au-TPP bonding. These gold states were also observed at similar energy windows in the PLDOS of the structures **1D**, **2D**, **4D**, **5D**, **3F**, and **3H** (see **Figure S3** in SI).

View Article Online
DOI: 10.1039/C7CP01440F

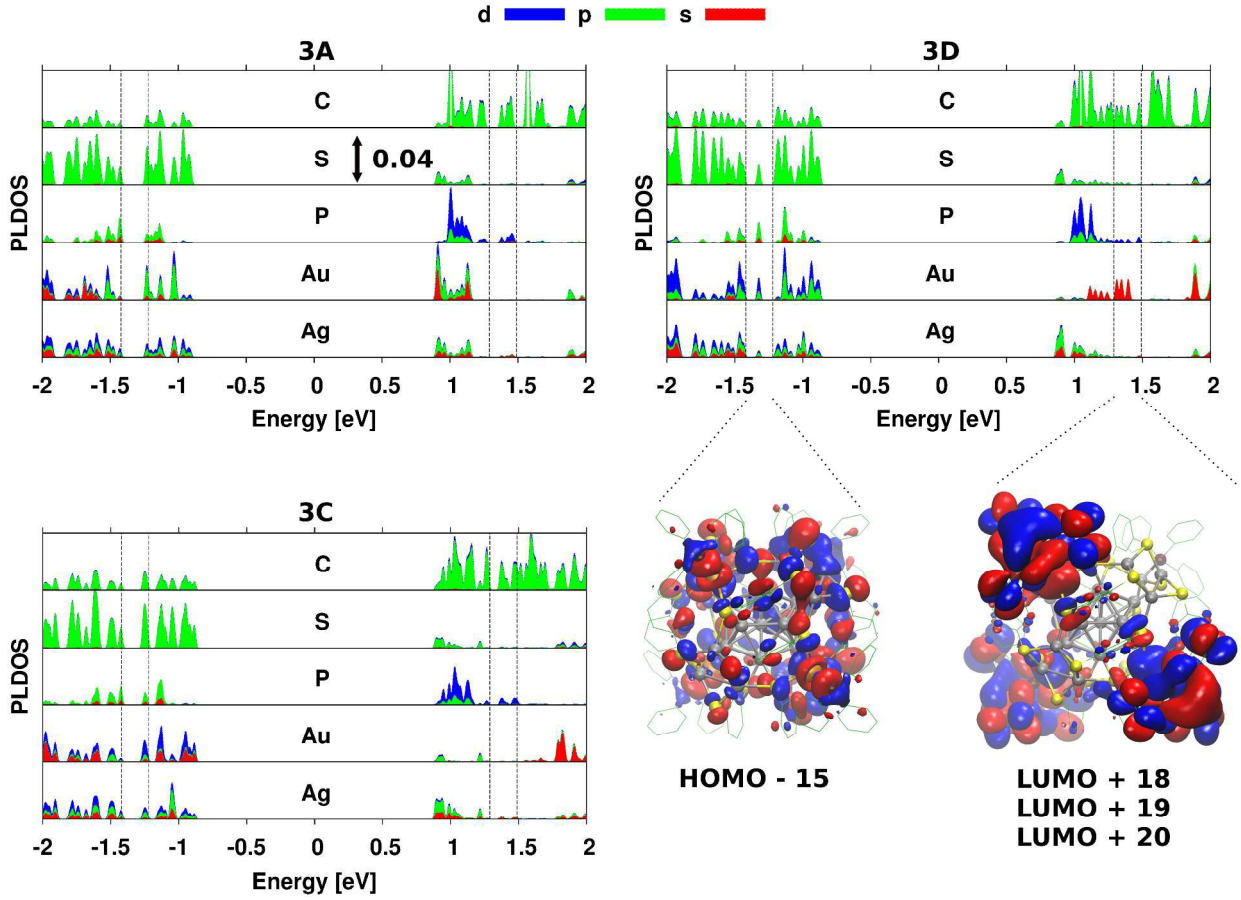

Figure 5. Angular-momentum-resolved (Y_{lm}) PLDOS per atom type (Ag, Au, P, S) and per phenyl ring (in the case of C) of the **3A**, **3C**, and **3D** structures. Blue, green, and red within the plots represent the density of the atomic s, p and d states. Dashed lines enclosure the occupied and unoccupied states around -1.32 eV and and 1.39 eV, respectively. Up-down arrow shows the Y_{lm} = 0.04 scale of each plot. At the bottom-right, the shape of the molecular orbitals of the **3D** structure located at -1.32 eV (HOMO - 15), and at 1.30 eV (LUMO + 18), 1.34 eV (LUMO + 19), and 1.39 eV (LUMO + 20).

In **Figure 5**, we also show the shape of the molecular orbitals of the **3D** nanocluster that appear at -1.32 eV and 1.30-1.39 eV, and that correspond to HOMO - 15 and LUMO + 18, LUMO + 19, and LUMO + 20. Note that for simplicity we draw the three unoccupied states in a single picture. The presence unoccupied states surrounding the nanocluster edges, where the Au-TPP bonds are located, also points out the importance of the Au-TPP bonding to determine electronic

View Article Online
DOI: 10.1039/C7CP01440F

transitions, and therefore, the optical properties of the thiolate-phosphine-protected $Ag_{29-x}Au_x$ materials.

CONCLUSIONS:

In this work, we show the importance of the bonding interaction between Au dopants and phosphine molecules in thiolate-phosphine-protected Ag nanoclusters. Particularly, we demonstrate that in the recently synthesized mixture of Au-doped $[Ag_{29-x}Au_x(BDT)_{12}(TPP)_4]^{3-}$ nanoclusters the interaction between Au-TPP play a crucial role in determining the cluster stability and electronic transitions. We show that the formation of Au-TPP bonds in the $[Ag_{29-x}Au_x(BDT)_{12}(TPP)_4]^{3-}$ structures could prevent the degradation of the cluster starting from the detachment of the phosphine molecules, since the Au-TPP bond is ~0.4 eV stronger than the analogous Ag-TPP one. Moreover, nanoclusters that have Au-TPP bonding exhibit an enhancement of the electronic transitions at ~450 nm, which is not observed in nanoclusters with pure Ag-TPP bonds. These electronic transitions, which involve the local p, d and s states of gold, explain the blue-shifting and broadening of the main absorption peak that has been experimentally observed in the synthesized mixture of products. We, moreover, suggest that the formation of Au-TPP bonds in the Au-doped nanoclusters could play a role in the enhancement of the photoluminescence quantum yield that has been experimentally observed. On the other hand, the small energy differences between the Au-doped isomers point out the importance of developing new strategies to produce (or isolate) the nanoclusters in which the Au dopants are strategically bonded to phosphine molecules.

ASSOCIATED CONTENT

View Article Online
DOI: 10.1039/C7CP01440F

Supplementary Information: Figures S1, S2, S3 and S4, Table S1 and Table S2.

AUTHOR INFORMATION

Corresponding Author

*E-mail: hannu.j.hakkinen@jyu.fi

Notes

The authors declare no competing financial interest.

ACKNOWLEDGMENTS

We thank Osman Bakr for providing the experimental crystal structures of the $[Ag_{29}(BDT)_{12}(TPP)_4]^{3-}$ and $[Ag_{28}Au(BDT)_{12}(TPP)_4]^{3-}$ nanoclusters, and Satu Mustalahti for useful discussions. This work is supported by the Academy of Finland (Project 294217 and H.H. Academy Professorship). The computational resources were provided by CSC-the Finnish IT Center for Science in Espoo, Finland.

REFERENCES

1 X. Ren, Z. Chen, X. Meng, D. Chen and F. Tang, *Chem. Commun.*, 2012, **48**, 9504–9506.

2 J. Zheng and R. M. Dickson, *J. Am. Chem. Soc.*, 2002, **124**, 13982–13983.

3 J. Yu, S. A. Patel and R. M. Dickson, *Angew. Chem. Int. Ed.*, 2007, **46**, 2028–2030.

4 N. Makarava, A. Parfenov and I. V Baskakov, *Biophys. J.*, 2005, **89**, 572–580.

5 C. I. Richards, S. Choi, J.-C. Hsiang, Y. Antoku, T. Vosch, A. Bongiorno, Y.-L. Tzeng and R. M. Dickson, *J. Am. Chem. Soc.*, 2008, **130**, 5038–5039.

View Article Online
DOI: 10.1039/C7CP01440F

6 T. Vosch, Y. Antoku, J.-C. Hsiang, C. I. Richards, J. I. Gonzalez and R. M. Dickson, *Proc. Natl. Acad. Sci.*, 2007, **104**, 12616–12621.

7 E. G. Gwinn, P. O'Neill, A. J. Guerrero, D. Bouwmeester and D. K. Fygenson, *Adv. Mater.*, 2008, **20**, 279–283.

8 J. T. Petty, J. Zheng, N. V Hud and R. M. Dickson, *J. Am. Chem. Soc.*, 2004, **126**, 5207–5212.

9 J. Yu, S. Choi and R. M. Dickson, *Angew. Chemie*, 2009, **121**, 324–326.

10 X. Yuan, Z. Luo, Y. Yu, Q. Yao and J. Xie, *Chem. Asian. J.*, 2013, **8**, 858–871.

11 J. Yu, S. Choi, C. I. Richards, Y. Antoku and R. M. Dickson, *Photochem. Photobiol.*, 2008, **84**, 1435–1439.

12 S. Choi, J. Yu, S. A. Patel, Y.-L. Tzeng and R. M. Dickson, *Photochem. Photobiol. Sci.*, 2011, **10**, 109–115.

13 Y. W. Zhou, C. M. Li, Y. Liu and C. Z. Huang, *Analyst*, 2013, **138**, 873–878.

14 Z. Wu, E. Lanni, W. Chen, M. E. Bier, D. Ly and R. Jin, *J. Am. Chem. Soc.*, 2009, **131**, 16672–16674.

15 O. M. Bakr, V. Amendola, C. M. Aikens, W. Wenseleers, R. Li, L. Dal Negro, G. C. Schatz and F. Stellacci, *Angew. Chem. Int. Ed.*, 2009, **48**, 5921–5926.

16 N. Cathcart, P. Mistry, C. Makra, B. Pietrobon, N. Coombs, M. Jelokhani-Niaraki and V. Kitaev, *Langmuir*, 2009, **25**, 5840–5846.

View Article Online
DOI: 10.1039/C7CP01440F

17 M. J. Alhilaly, M. S. Bootharaju, C. P. Joshi, T. M. Besong, A.-H. Emwas, R. Juarez-Mosqueda, S. Kaappa, S. Malola, K. Adil, A. Shkurenko, H. Häkkinen, M. Eddaoudi and O. M. Bakr, *J. Am. Chem. Soc.*, 2016, **138**, 14727–14732.

18 H. Yang, J. Lei, B. Wu, Y. Wang, M. Zhou, A. Xia, L. Zheng and N. Zheng, *Chem. Commun.*, 2013, **49**, 300–302.

19 H. Yang, J. Yan, Y. Wang, H. Su, L. Gell, X. Zhao, C. Xu, B. K. Teo, H. Häkkinen and N. Zheng, *J. Am. Chem. Soc.*, 2017, **139**, 31–34.

20 L. G. AbdulHalim, M. S. Bootharaju, Q. Tang, S. Del Gobbo, R. G. AbdulHalim, M. Eddaoudi, D. Jiang and O. M. Bakr, *J. Am. Chem. Soc.*, 2015, **137**, 11970–11975.

21 G. Soldan, M. A. Aljuhani, M. S. Bootharaju, L. G. AbdulHalim, M. R. Parida, A.-H. Emwas, O. F. Mohammed and O. M. Bakr, *Angew. Chem. Int. Ed.*, 2016, **55**, 5749–5753.

22 Y. Wang, S. Curtarolo, C. Jiang, R. Arroyave, T. Wang, G. Ceder, L.-Q. Chen and Z.-K. Liu, *Calphad*, 2004, **28**, 79–90.

23 C. Wang, H. Wang, T. Huang, X. Xue, F. Qiu and Q. Jiang, *Sci. Rep.*, 2015, **5**, 10213-1–11.

24 B. Zhou and E. A. Carter, *J. Chem. Phys.*, 2005, **122**, 184108-1–10.

25 L. F. L. Oliveira, N. Tarrat, J. Cuny, J. Morillo, D. Lemoine, F. Spiegelman and M. Rapacioli, *J. Phys. Chem. A*, 2016, **120**, 8469–8483.

26 X. Huang, S. Li, Y. Huang, S. Wu, X. Zhou, S. Li, C. L. Gan, F. Boey, C. A. Mirkin and H. Zhang, *Nat. Commun.*, 2011, **2**, 292-1–6.

View Article Online
DOI: 10.1039/C7CP01440F

27 M. Walter, J. Akola, O. Lopez-Acevedo, P. D. Jadzinsky, G. Calero, C. J. Ackerson, R. L. Whetten, H. Grönbeck and H. Häkkinen, *Proc. Natl. Acad. Sci. USA*, 2008, **105**, 9157–9162.

28 J. Enkovaara, C. Rostgaard, J. J. Mortensen, J. Chen, M. Dułak, L. Ferrighi, J. Gavnholt, C. Glinsvad, V. Haikola, H. A. Hansen, H. H. Kristoffersen, M. Kuisma, A. H. Larsen, L. Lehtovaara, M. Ljungberg, O. Lopez-Acevedo, P. G. Moses, J. Ojanen, T. Olsen, V. Petzold, N. A. Romero, J. Stausholm-Møller, M. Strange, G. A. Tritsaris, M. Vanin, M. Walter, B. Hammer, H. Häkkinen, G. K. H. Madsen, R. M. Nieminen, J. K. Nørskov, M. Puska, T. T. Rantala, J. Schiøtz, K. S. Thygesen and K. W. Jacobsen, *J. Phys. Condens. Matter.*, 2010, **22**, 253202-1–24.

29 J. J. Mortensen, L. B. Hansen and K. W. Jacobsen, *Phys. Rev. B*, 2005, **71**, 35109-1–11.

30 J. P. Perdew, K. Burke and M. Ernzerhof, *Phys. Rev. Lett.*, 1996, **77**, 3865–3868.

31 M. Dion, H. Rydberg, E. Schröder, D. C. Langreth and B. I. Lundqvist, *Phys. Rev. Lett.*, 2004, **92**, 246401-1–4.

32 M. Dion, H. Rydberg, E. Schröder, D. C. Langreth and B. I. Lundqvist, *Phys. Rev. Lett.*, 2005, **95**, 109902–1.

33 M. E. Casida, C. Jamorski, F. Bohr, J. Guan and D. R. Salahub, *Recent Adv. Funct. Methods; ACS Press Washington, D.C.*, 1996, 145.

34 M. Walter, H. Häkkinen, L. Lehtovaara, M. Puska, J. Enkovaara, C. Rostgaard and J. J. Mortensen, *J. Chem. Phys.*, 2008, **128**, 244101-1–10.

35 X. Andrade, S. Botti, M. A. L. Marques and A. Rubio, *J. Chem. Phys.*, 2007, **126**,

View Article Online
DOI: 10.1039/C7CP01440F

184106-1–8.

36 S. Malola, L. Lehtovaara, J. Enkovaara and H. Häkkinen, *ACS Nano*, 2013, **7**, 10263–10270.

37 G. Henkelman, A. Arnaldsson and H. Jónsson, *Comput. Mater. Sci.*, 2006, **36**, 354–360.

38 D. Otálvaro, T. Veening and G. Brocks, *J. Phys. Chem. C*, 2012, **116**, 7826–7837.